Thermo-economic analysis and multi-objective optimisation of lignocellulosic biomass conversion to Fischer-Tropsch fuels

Electronic Supplementary Information

Emanuela Peduzzi[a,*], Guillaume Boissonnet[b], Geert Haarlemmer[b], François Maréchal[a]

[a] *Ecole Polytechnique Fédérale de Lausanne*
Industrial Process and Energy Systems Engineering
Rue de l'Industrie 17, Case Postale 440, CH-1951 Sion, Switzerland
[b] *CEA - Grenoble DRT/LITEN/DTBH/*
Laboratoire des Technologies de Conversion de la Biomasse
17 rue des Martyrs 38054 GRENOBLE cedex 9, France

Nomenclature

1. Appendix A: Process modelling

This section reports the modelling of Biomass to Liquids (BTL) conversion processes both in terms of thermochemical models and process integration. The models developed to represent the Fast Internally Circulating Fluidised Bed (FICFB) gasification and HighâĄżTemperature Electrolysis (HTE) are presented in detail, whereas all other models used are summarised and referenced at the end of this Section.

1.1. Process integration

The objective of the process integration of the BTL plants is to optimise the production of fuel and co-production of electricity, calculating feasible energy targets. The optimisation problem aims at minimising the costs associated with the inputs (such as biomass and electricity), minus the revenues associated with the output streams (such as Fischer-Tropsch (F-T) and electricity). The constraints of the problem are represented by the mass balances between the units, the heat

*corresponding author: ep@emanuelapeduzzi.com

cascade (which is the heat balance per temperature interval and of the overall process) and the unit selected from to the superstructure. Steam turbines and heat pumps can also be introduced as optional energy recovery systems (through integer variables). The heat requirement (hot utility) is provided by the combustion of the off-gases from the process. If this is not sufficient, selected process streams can be used as fuel to close the balance, through reducing the flows of the main conversion process. The cooling requirement (cold utility) is provided by conventional cooling using river water.

The process integration model is formulated as a Mix integer linear programming (MILP) optimisation problem and is described in [1, 2, 3, 4]. The heat transfer between streams is assured by considering an appropriate ΔT_{min}. The relationship between the $\Delta T_{min}/2$, assigned to each stream (j), and the corresponding heat transfer coefficient (α), is reported in Equation 1 according to the empiric correlation proposed by [1].

$$\Delta T_{min,j}/2 = \Delta T_{min,ref}/2 \cdot \left(\frac{\alpha_{ref}}{\alpha_j}\right)^b \tag{1}$$

Where α_{ref} and $\Delta T_{min,ref}$ are the heat transfer coefficient and minimum approach temperature of a reference heat exchanger.

As a simplifying assumption, four types of (heat) streams are considered and to each type a different value of $\Delta T_{min}/2$ is assigned. The types are defined as liquids, gases, phase changing streams, and reactors. For continuity with previous studies, the same assumptions used by [1] and [5] are used here. The $\Delta T_{min}/2$ and corresponding heat transfer coefficient, for each type of stream, are summarised in Table 1.

Table 1: $\Delta T_{min}/2$ and corresponding heat transfer coefficient, considering $\alpha_{ref} = 580\ W/m^2K$ and $\Delta T_{min,ref} = 10\ K$ (adapted from [1])

Stream type	$\Delta T_{min}/2$ $[K]$	α $[W/m^2K]$
phase change	2	1823
liquid	4	767
gas	8	322
reactors	25	78

The value of $\Delta T_{min,ref}$ represents a compromise between the heat exchangers' surface area

required to satisfy the energy target, which affects the investment cost, and the heat that is recovered from the process, which affects the energy conversion efficiency. If each value α_j is fixed, the corresponding $\Delta T_{min,j}/2$ can be considered variable. $\Delta T_{min,ref}$ can therefore be optimised by considering it as a decision variable in the master problem.

1.2. Fluidised bed gasification

Gasification is a complex process and accurate models should take into account a large number of species and reactions [6], but such models are beyond the scope of this study and would not be appropriate in the context of process design [1]. In the context of thermo-economic modelling of BTL processes Entrained Flow (EF) gasification is generally represented using equilibrium models, justified by the high temperature achieved in the process, whereas several different solutions to model FICFB are proposed in the literature, beyond using fixed operating points and conversion reactions. Some authors use equilibrium models [7, 8] even though, in practice it is difficult to reach equilibrium for solid carbon gasification below 1000 ℃ as discussed by [9]. Therefore, corrections to the equilibrium have been introduced, for example, by using conversion factors to represent char methane and higher hydrocarbon yields [10], by adjusting the equilibrium constant using a multiplication factor [11], and by using a combination of both approaches [12]. Another approach to modify the equilibrium constant is to introduce a temperature difference to the equilibrium. This approach was first introduced by [13] and used to model gasification processes by [9].

The model proposed in this study is based on experimental data obtained at the Laboratoire Technologies Biomasse (LTB) fludized bed gasification facility and stems from the FICFB model previously developed by [14]. This model is based on both pseudo-equilibrium equations through temperature differences, to predict the major gas composition, and conversion factors, to take into account the char and higher hydrocarbon yield. The model is built on the basis of gasification experiments in the fluidised bed gasifier facility at LTB. The facility is described by [15]. It should be underlined however that the results were obtained in the context of previous work, therefore the experiments were not designed for the purpose of this study and in the frame of proposing a gasification model. Nevertheless, it was possible to build a coherent model fitting the data points available. The model parameters are obtained through data validation and reconciliation using the

software Vali® by [16]. The resulting model is simple for fast resolution and easy implementation. It allows calculating the gas composition and char conversion, given the input biomass composition and the main operating conditions: S/B and T_g

1.2.1. Gasification model

The overall structure of the model is summarised in Figure 1, where the input parameters and output variables of interest for the model are specified. This figure also highlights the gases that are experimentally measured in fluidised bed gasification.

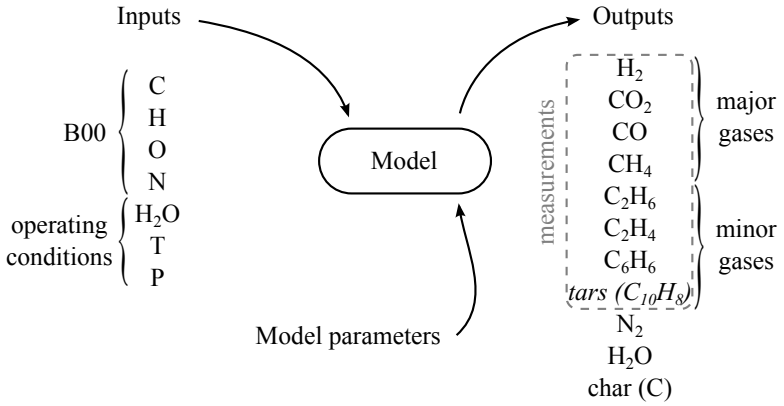

Figure 1: Representation of the model structure, including inputs and outputs, and gases measured (tars are represented by a single molecule for simplicity, in reality several molecules are measured).

This study proposes a set of equations representing the gasification model, and a set of parameters, *a priori* function of the main operating conditions, for resolution.

The main underlying and simplifying assumptions considered are summarised hereafter:

- A short residence time: tar cracking reactions are not taken into consideration;
- A homogeneous process: temperature gradients, heat and mass transfer mechanisms, hydrodynamics are not taken into consideration;
- The S/B is higher than ~0.5 [1];
- Heavier tars are represented by naphthalene, $C_{10}H_8$;
- Char is represented by pure carbon.

[1] This constraint is set by the range of the data available.

The gasification facility consists of a fluidised bed with a feeding rate of 0.5-4 kg/h, designed to study biomass steam gasification up to 1000 ℃ and 40 bar. Gas composition is analysed online using a micro Gas Chromatograph, coupled with a Thermal Conductivity Detector, as explained by [15]. The data considered was acquired averaging the experimental results obtained between 30 minutes and one hour after the beginning of biomass injection. The gas composition and production, in this time frame, in fact, were shown to be similar to the results of the Güssing FICFB gasifier pilot facility [17, 18]

1.2.2. Gasification model equations

The analysis of the problem, as presented in Figure 1, results in seven degrees of freedom, calculated from the difference between the number of independent variables (considering Gibbs' phase rule) and the number of equations available (considering mass, impulse and energy balances). This means that there are seven more unknowns than equations, therefore seven model equations need to be defined to obtain a determined system. The major gases, H_2, CO, CO_2, and CH_4, are represented by pseudo-equilibrium reactions, for which a temperature difference ΔT_{eq} to the equilibrium is introduced. Given a general reaction in the form of Equation 2, the apparent equilibrium constant $\hat{K}_{eq}$, can be expressed by Equation 3. $\hat{K}_{eq}$ is a function of the equilibrium constant K_{eq} and, neglecting deviations from ideal behaviour, of the concentrations of reactants and reagents $[X]$ observed.

$$\alpha A + \beta B \rightleftharpoons \rho R + \sigma S \tag{2}$$

$$\hat{K}_{eq} = K_{eq}(T_g + \Delta T_{eq}) = e^{-\frac{\Delta G^o}{R\cdot(T+\Delta T_{eq})}} = \frac{[R]^\rho [S]^\sigma}{[A]^\alpha [B]^\beta} P^{\rho+\sigma-\alpha-\beta} \tag{3}$$

Where P is system pressure.

The set of independent reactions taken into consideration are the water gas shift and the steam methane reforming reactions (Equations 4 and 5), reported in Table 2.

Table 2: Reactions considered in the gasification model

	reaction	$\Delta H_R^0 [kJ/mol]$	
Water gas shift (WGS)	$CO + H_2O \rightleftharpoons CO_2 + H_2$	-41	(4)
Steam methane reforming (SMR)	$CH_4 + H_2O \rightleftharpoons CO + 3H_2$	+206	(5)

As in the model by [14], the remaining components are modelled using conversion equations. This is because the minor gases concentrations observed are far from the equilibrium, and char would be represented only implicitly by equilibrium reaction. Therefore, in order to improve the robustness of the model, equilibrium reactions are used only to represent the major gases [14]. Equation 6 represents the conversion of carbon present in the initial biomass into char. Minor gaseous components are represented by Equations 7, 8, 9 and tar by Equation 10.

$$char\ conversion: \ Char = C_{B00} \cdot (1 - \epsilon_{c_C}) \tag{6}$$

$$ethylene\ conversion: \ \tilde{G}_{C_2H_4} = \tilde{C}_{B00} \cdot \tilde{\epsilon}_{c_{C_2H_4}} \tag{7}$$

$$ethane\ conversion: \ \tilde{G}_{C_2H_6} = \tilde{C}_{B00} \cdot \tilde{\epsilon}_{c_{C_2H_6}} \tag{8}$$

$$benzene\ conversion: \ \tilde{G}_{C_6H_6} = \tilde{C}_{B00} \cdot \tilde{\epsilon}_{c_{C_6H_6}} \tag{9}$$

$$tar\ conversion: \ \tilde{G}_{tar} = \tilde{C}_{B00} \cdot \tilde{\epsilon}_{c_{tar}} \tag{10}$$

Where $\tilde{\epsilon}_{c_x}$ represents the molar ratio between the moles produced of compound x and the moles of carbon in the initial biomass. For char the ratio is expressed on a mass basis.

1.2.3. Gasification model parameters

The model parameters, which are the temperature differences to equilibrium ΔT_{eq} and the conversion factors ϵ_x, are determined on the basis of four datasets relative to four gasification experiments carried out in the fluidised bed at LTB. For each dataset the information available consists of:

- The ultimate analysis, humidity Φ, and biomass type (agropellets (calys) and beech wood);
- The S/B, steam to biomass ratio [2];
- The major and minor gas yield in mol/mol$_{B00_{C6}}$;
- The gasification temperature T_g, ranging from 750 ℃ to 875 ℃;
- The gasification pressure, which has been considered constant at 1 bar for simplicity.

The methodology used to determine the model parameters is based on data validation and reconciliation. This technique takes into account the level of accuracy associated with experimental measurements to build a consistent set of data and give the most likely and coherent representation of the system. In this study, the data validation and reconciliation algorithm of the software Vali® by [16], is used to reconcile the experimental data relative to the composition of the synthesis gas and, simultaneously, to estimate model parameters that best fit the experimental data. The data validation and reconciliation problem can be expressed as a constrained optimisation problem in the form of Equations 11, 12 and 13:

$$min \sum_i \left(\frac{y_i - y_i^*}{\sigma(y_i)} \right)^2 \tag{11}$$

subject to:

$$F(y_i^*, x_j) = 0; \tag{12}$$

$$G(y_i^*, x_j) > 0; \tag{13}$$

Where y_i represents the values measured, y_i^* the reconciled values and $\sigma(y_i)$ the accuracies of the measurements. The system of equations representing the model is expressed by F, and the

[2]Where steam is the total amount of water that enters the gasifier, it includes both the steam injected in the gasifier and water in biomass in the form of moisture. Biomass is intended as $B00$, therefore on a dry basis (db).

Table 3: Accuracy imposed on the experimental results for data validation and reconciliation

Measured gas	Accuracy
H_2	5%
CO	5%
CO_2	5%
CH_4	5%
C_2H_4	50%
C_2H_6	50%
C_6H_6	50%
Tar ($C_{10}H_8$)	50%

inequality constraints, by G. In the present study x_j represents both the non-measured variables, which need to be calculated, and the model parameters, which also need to be determined.

Considering the eight experimental values, relative to the gas composition, which are available from each experimental run, a maximum number of eight parameters (for a maximum number of eight equations) can be estimated. As said earlier, nevertheless, seven equations are sufficient to obtain a determined system for which seven parameters need to be estimated. The accuracy assigned to the values measured to solve the data validation and reconciliation problem, and reported in Table 3, are not experimental accuracies. In this case, and for the sole purpose of developing a model, they represent a measure of the accuracy desired from the model for the representation of the experimental values. That is, the major gases are to be determined with the highest accuracy with respect to the experimental values, whereas minor gases can be estimated with less stringent accuracy. Tars, which are represented by a single molecule in the model, have therefore the least stringent requirements.

The model parameters obtained from the resolution of the data reconciliation problem, for each one of the four experimental data sets, are presented in Figures 2, 3, 4. These figures also present the regressions for each parameter as a function of temperature, the corresponding equations are presented in Table 4. The parameters are represented and evaluated as a function of temperature because, given the range and number of the experimental data available, it was not possible to directly establish the effect of the S/B ratio on the model parameters. The values obtained for the model parameters, in fact, are not statistically correlated to the S/B ratio (by multivariate regression analysis).

The values obtained for the ΔT_{eq} are presented in Figure 2. As expected, the ΔT_{eq} is positive for

the exothermic reaction, that is the water gas shift (4) and negative for the endothermic reaction, that is the steam methane reforming (5). The reactants concentrations for an exothermic reaction, which is not at equilibrium, in fact, correspond to an apparent equilibrium constant ($\hat{K}_{eq}$, from Equation 3) at a temperature higher than the measured one, vice versa for an endothermic reaction the temperature is lower than the measured one. Figure 2 shows that the ΔT_{eq} for the water gas shift reaction decreases with temperature, which indicates that at higher temperature the water gas shift tends to equilibrium. Above 850 °C there seems to be a change of the slope of this trend, therefore, the regression was carried out in two steps (and constrained on the value of ΔT_{eq} estimated at 850 °C). More experimental data would be required for a better fit of the estimated parameter. ΔT_{eq} for the steam methane reforming reaction, on the contrary, varies much less with temperature and becomes slightly more negative as the temperature increases. Methane in gasification is produced also in the pyrolysis phase which may explain this unexpected trend. Also in this case, more experimental data would provide useful information for a better understanding and estimation of this parameter.

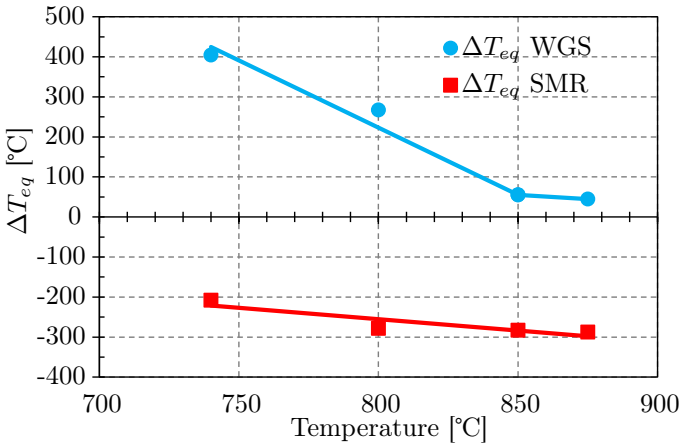

Figure 2: Major gas conversion

The values estimated for the minor gases conversion parameters $\tilde{\epsilon}_x$ are reported in Figure 3. The general trend is the reduction of the conversion factors with temperature. This trend was not clear in regard to the production of benzene, therefore, for this molecule, an average value of the conversion factor over the temperature range was considered, instead of a regression. The regressions for the conversion factors are reported in Table 4.

The char conversion ϵ_{char} during gasification, as expected, increases with temperature as shown

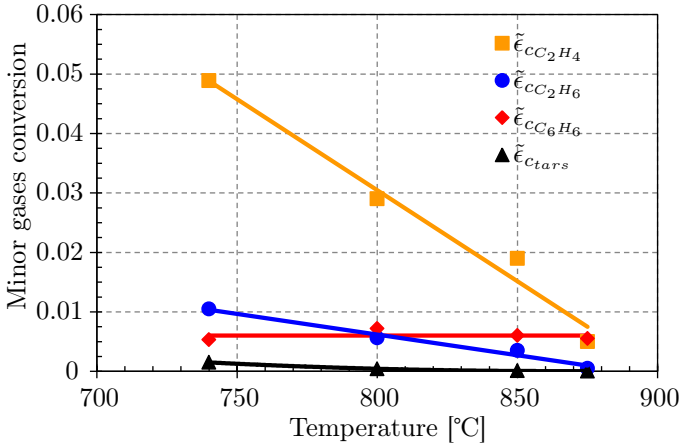

Figure 3: Minor gas conversion

in Figure 4. In this case a quadratic regression was used to represent the estimated parameter as a function of temperature. It should be underlined that the residual char is oxidised in the combustion chamber to provide the heat necessary to the gasification reaction, should this not be sufficient, an additional fuel would be required to sustain the process.

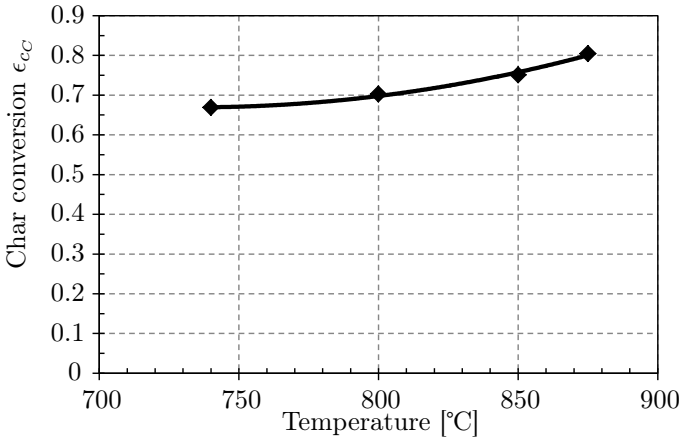

Figure 4: Carbon conversion

The correlations obtained by the regressions of the model parameters as a function of temperature are summarised in Table 4, where the corresponding coefficients of determination are also reported, when relevant.

1.2.4. Gasification model results

The model equations and the model parameters (as a function of temperature) presented are the basis of the FICFB model proposed in this study. Figures 5 and 6, show how the model results, for the major and minor gases respectively, compared to the experimental data of the fluidised bed

Table 4: Model parameters' correlations

Parmeter	Correlation[a]	R^2	
ΔT_{eq} water gas shift [°C][b]	$= -3.3596 \cdot T - 2910.50$	0.96	(14)
ΔT_{eq} steam methane ref. [°C]	$= -0.5680 \cdot T - 199.01$	0.81	(15)
$\tilde{\epsilon}_{c_{C_2H_4}}$ [$mol_{C_2H_4}/mol_{C_{B00}}$]	$= -0.0003 \cdot T + 0.2753$	0.98	(16)
$\tilde{\epsilon}_{c_{C_2H_6}}$ [$mol_{C_6H_6}/mol_{C_{B00}}$]	$= -6.9643E^{-5} \cdot T + 0.0619$	0.98	(17)
$\tilde{\epsilon}_{c_{C_6H_6}}$ [$mol_{C_6H_6}/mol_{C_{B00}}$]	$= 6.026E^{-3}$	-	(18)
$\tilde{\epsilon}_{c_{tars}}$ [$mol_{C_6H_6}/mol_{C_{B00}}$]	$= 1.298E^{6} \cdot e^{-0.0276 \cdot T}$	0.99	(19)
ϵ_{c_C} [g/g]	$= 6.629E^{-6} \cdot T^2 - 9.738E^{-4} \cdot T + 4.246$	0.99	(20)

[a] Temperature in °C.
[b] Correlation relative to $T < 850$ °C.

gasifier facility at LTB. Given the small number of data points available for this study, the data presented is the same that is used for the calibration of the model parameters.

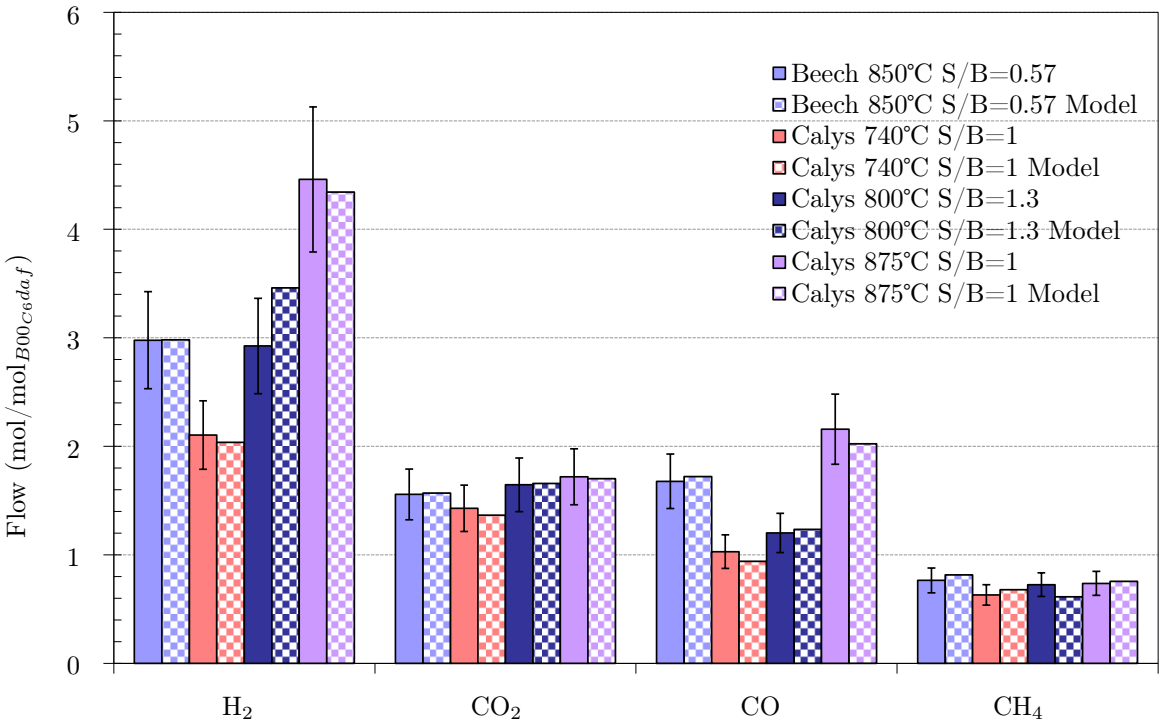

Figure 5: Comparison of model and experimental results for the major gases

The major gases, presented in Figure 5, are reproduced generally within 15% of the values observed. The error bar for the minor gases, presented in Figure 6, is more important. Minor gases and tars are generally predicted within 50% error. The main component of the higher hydrocarbons is ethylene, which is compatible with the gas chromatography results of the analysis carried out at

Güssing ([19]).

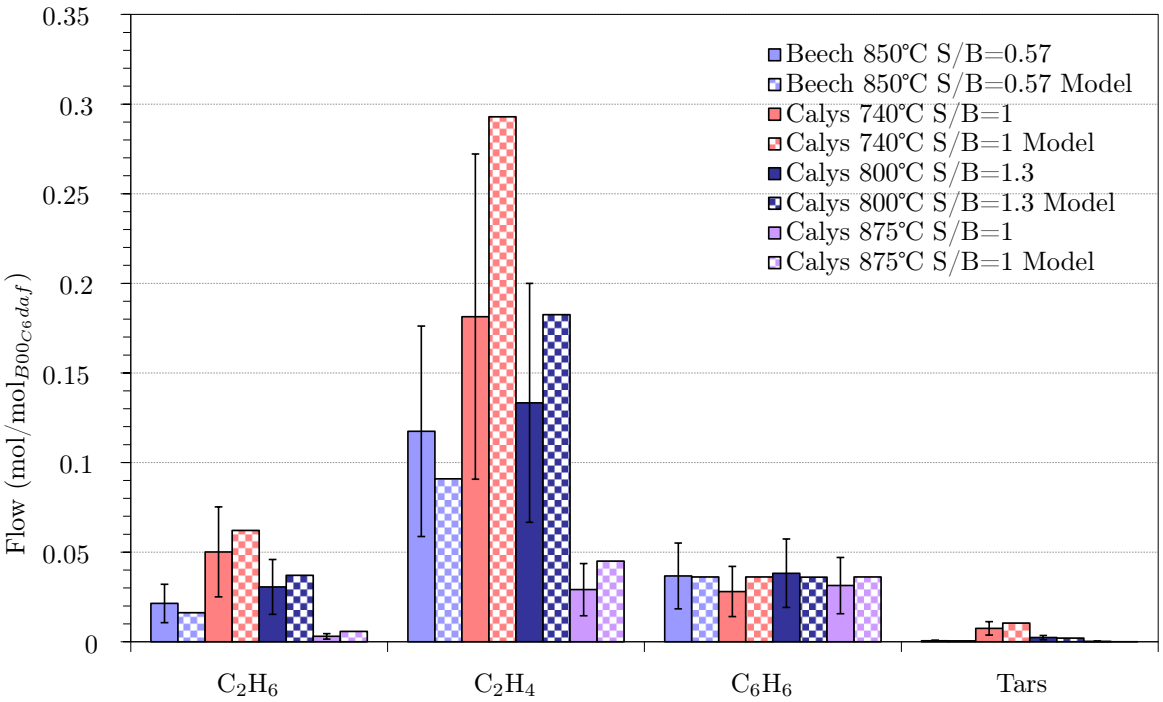

Figure 6: Comparison of model and experimental results for the minor gases

Figure 7 reports the model results as a function of temperature for two S/B ratios, 0.5 and 0.9. The same figure also reports the gas composition measured in the industrial scale plant at Güssing, at a temperature of 850 ℃and S/B ratio ranging from 0.6 and 0.8 ([17]). The model results are obtained, for comparison, considering the same biomass composition and humidity reported by [17]. The model predicts the gas concentrations within the range of the literature values, though CO and C_2H_4 are underestimated.

The trends displayed in Figure 7, in terms of gas composition as a function of the S/B ratio, are compatible with the results reported by [19] from the Güssing FICFB gasifier. The data reported by [19] shows that H_2 and CO_2 concentration increase with the S/B ratio, whereas CO, CH_4 decrease. The trends as a function of temperature, in terms of the main gases, are compatible for H_2, CO (increasing with temperature) and CO_2 (decreasing with temperature). For CH_4 though, the model, predicts a concentration close to the experimental values, but shows a slight increase in concentration with temperature. The experimental results from Güssing's plant show a slight decrease instead. This is due to the correlation obtained for the ΔT_{eq} of the steam methane reforming reaction (Equation 15), for which more experimental results would be required.

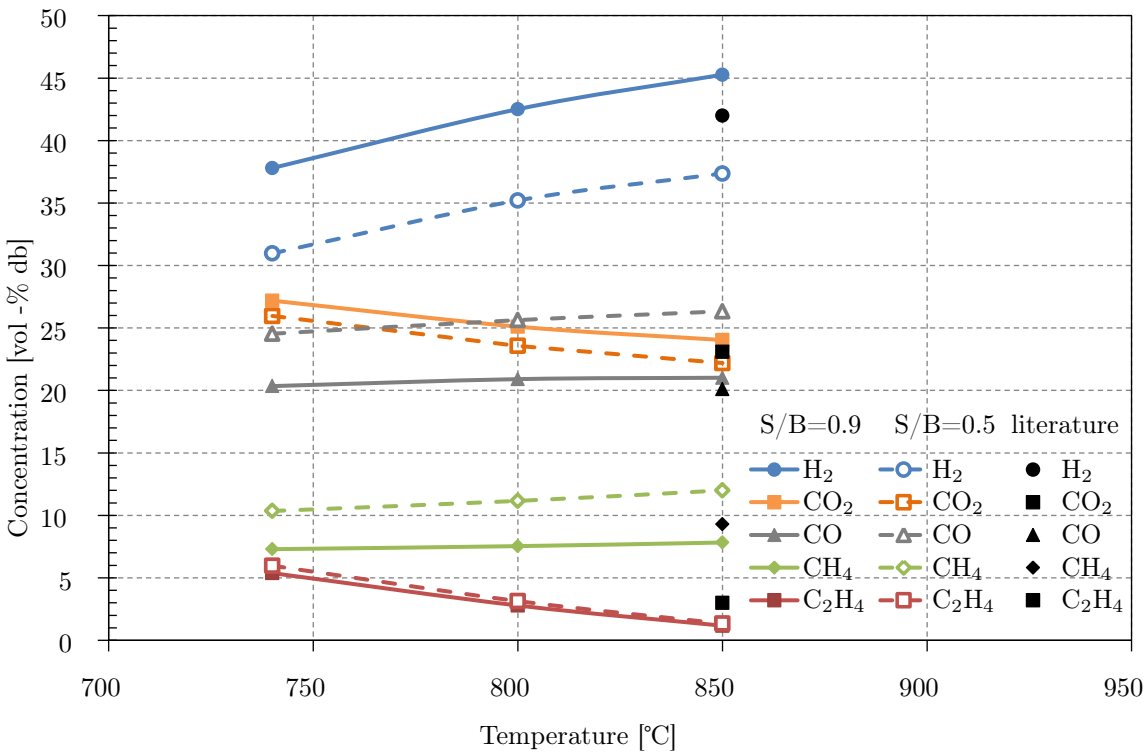

Figure 7: Model results as a function of temperature for S/B ratios, 0.5 (solid) and 0.9 (dashed).

Nevertheless, as the variation of concentration for CH_4 is small, in comparison to that of other gases, and the values predicted are in the same range as the experimental values, the model may be considered sufficiently accurate in the context of this study. Further modelling aspects that should be addressed are:

- The evaluation of the effect of S/B ratio on model parameters, especially for values below 0.5;
- The improvement of the representation of CH_4 yield through a better estimation of the ΔT_{eq} relative to the steam methane reforming reaction;
- A rigorous model validation.

This model represents the basis for the thermochemical representation of biomass gasification in an FICFB gasifier, in the context of the techno-economic evaluation and optimisation of BTL process chains.

1.3. Electrolysis and co-electrolysis

H_2 produced by high temperature steam electrolysis, in a solid oxide electrolyser cell (SOEC), can be added to achieve the desired H_2/CO as an alternative to the Sater Gas Shift (WGS)

unit operation. This unit operation can optionally be considered for only steam electrolysis or steam/CO_2 co-electrolysis using, in the latter case, CO_2 recycled from the Acid Gas Removal (AGR).

The overall reaction to produce a synthesis gas with a H_2/CO of 2 through co-electrolysis of H_2O and CO_2 can be written as Equation 21:

$$CO_2 + 2H_2O \overset{electricity+heat}{\longrightarrow} CO + 2H_2 + 3/2O_2 \tag{21}$$

The total energy required to split H_2O and CO_2 (ΔH) is composed of electrical (ΔG) and thermal energy ($T\Delta S$). The interest of high temperature electrolysis lies in the fact that with temperature, above 100 ℃, the total energy remains essentially unchanged, whereas the (minimum) contribution of electricity (ΔG) declines significantly and the (maximum) contribution of heat ($T\Delta S$) increases.

This feature shows, on the one hand, the potential of SOEC to reduce the specific electricity requirement in comparison to technologies using alkaline and proton exchange membrane electrolytes, which operate at low temperatures. On the other hand, it shows the potential for integration with the rest of the BTL process to satisfy the heat requirement of the unit.

1.3.1. Electrolysis model

The model proposed to represent high temperature electrolysis and co-electrolysis in a SOEC is developed on the basis of the work by [20, 21] on a solid oxide fuel cell (SOFC). The operation of an electrolysis cell, in fact, is reversed with respect to that of a fuel cell. In a SOFC O_2 is reduced at the cathode, the O^{2-} anions migrate through the solid oxide electrolyte and the 'fuel' (H_2 for example) is oxidised at the anode inducing an electrochemical potential across the electrodes. The same equations and general principles, with the necessary adjustments, can be used to represent a SOEC and a SOFC. The limitation of this model is that the model parameters to calculate the ASR were evaluated for conditions relative to a SOFC (fuelled with biogas). Here they are applied in a different context. Without experimental data relative to the operation the SOFC in

regenerative mode, as a SOEC, the values of these parameters remain the best possible estimate in the context of this study.

Only the main equations of the model by [20, 21] are presented here, adapted to represent **steam electrolysis**.

Supposing isothermal operation under constant current density the main model parameters are:

- the current density j, 0.3 A/cm^2;
- the area of each cell A_{cell}, 200 cm^2;
- the molar flow of H_2, $\dot{n}_{H_2}$, which is determined by the composition of the synthesis gas and, in the case of co-electrolysis, the amount of CO_2 fed to the SOEC;
- the molar flow of CO_2, $\dot{n}_{CO_2}$, for co-electrolysis, which depends on the fraction recycled from the AGR unit: R_{CO_2};
- the stack temperature T_{soec};

For each mole of H_2 required by the process 0.5 moles of O_2 are produced by steam electrolysis, the flow of O_2, $\dot{n}_{O_2}$, can be related to the current flowing through the SOEC by Faraday's law of electrolysis:

$$\dot{n}_{O_2} = \frac{j \cdot A_{cell} \cdot N_{cells}}{4F} = \frac{I \cdot N_{cells}}{4F} \tag{22}$$

From which the total number of cells in the stack, N_{cells} can be computed, and therefore the total area of the stack A_{stack}:

$$A_{stack} = A_{cell} \cdot N_{cells} \tag{23}$$

As said earlier, the electric power required to operate the stack needs to be determined by taking into account ohmic, diffusion and activation losses. The total electric power, W_{el}, required to operate the SOEC is therefore computed by Equation 24.

$$W_{el} = \Delta G + W_{losses} = \Delta G + R_{ohmic,stack} \cdot I^2 + (\eta_{cathode} + \eta_{anode}) \cdot N_{cells} \cdot I \tag{24}$$

The relationships and constants used to calculate the terms relative to ohmic ($R_{ohmic,stack}$) and non-ohmic ($\eta_{cathode} + \eta_{anode}$) losses are described in detail by [21].

From W_{el} it is possible to obtain the operating voltage of the stack according to Equation 26.

$$V_{stack} = \frac{W_{el}}{I} \tag{25}$$

$$V_{cell} = \frac{V_{stack}}{N_{cells}} \tag{26}$$

When the SOEC is used for **co-electrolysis** and CO_2 is added to the feed, the amount of CO produced is obtained by considering the RWGS at equilibrium at the cathodes outlet. As discussed earlier, the RWGS reaction seems to provide the most important contribution to the production of CO from CO_2 ([22, 23]).

1.4. Models summary

Tables 1.4 and 1.4 summarise the models of the unit operations used to convert biomass into synthesis gas and the ones used to convert synthesis gas into the final F-T fuel.

Table 5: Biomass conversion modelling summary

Unit	Description
Biomass	Composition: 50.81% carbon, 5.96% hydrogen, 43.05% oxygen, 0.18% nitrogen, wood type. Lower Heating Value (LHV) and Higher Heating Value (HHV) modelled according to Boie's equation [24] by the definition of the enthalpy of formation of *pseudo-compounds* corresponding to the elemental constituents of biomass. The LHV on a dry basis corresponds to 18.73 MJ/kg. Raw biomass moisture content (MC) is set to 35%. The value of the enthalpy of formation of bound water neglected as the models used for drying are calibrated without considering this parameter. The Gibbs free energy of biomass is also not taken into account in the model. The biomass model is described in detail in [25].

Unit	Description
Air drying	Model described in detail by [14]. The sorption isotherm of the wood surface-air system at equilibrium is described by $\Phi = 2.865 \cdot 10^{-2}\phi_{air}^{1/2} + 2.307 \cdot 10^{-1} - 1.273 \cdot 10^{-3}(T - 273))\phi_{air} - 2.519 \cdot 10^{-1}\phi_{air}^{2} + (2.199 \cdot 10^{-1} + 8.630 \cdot 10^{-4}(T - 273))\phi_{air}$; where ϕ_{air} is the air relative humidity (%), Φ is the biomass relative humidity (kg_{H_2O} kg_{tot}^{-1}), and T is air temperature in K. In order to take into account that equilibrium is not reached, the amount of water that evaporates, $\dot{m}_{H_2O,vap}$ in kg/s, is calculated in analogy to the heat transfer in a heat exchanger by $\frac{\dot{m}_{H_2O,vap}}{\dot{m}_{air}} = U_p \Delta p_{lm}$; where U_p is an overall mass transfer coefficient calibrated to $11.16 \cdot 10^{-3} bar^{-1}$ and Δp_{lm} is the log-mean partial pressures difference between the inlet and outlet of the dryer
Steam drying	Model described in detail by [14]. The drying process is controlled by the heat transfer, there, as in the air dryer case, the amount of steam required to evaporate the moisture can be calculated by $\frac{\dot{m}_{H_2O,vap}\Delta h_{vap}}{\dot{m}_{steam}} = U_T \Delta T_{lm}$; where U_T is an overall heat transfer coefficient calibrated to 1117 J $kg^{-1}K^{-1}$ and ΔT_{lm} is the log-mean temperature difference between the inlet and outlet of the dryer
Torrefaction	Solid product composition and gaseous yield heating value are represented as a function of the Anhydrous Weight Loss (AWL) and torrefaction temperature (T_{torr}) as described in [26]. The heat requirement for the evaporation of residual moisture, after drying, is considered to be double that of water. Torrefaction is modelled as an indirectly heated reactor and the gases produced are combusted for heat.
Grinding[a]	The electricity consumption for fine grinding of biomass into particles suitable for EF gasification (~200 µm) is assumed to be 500 kWh/t for raw biomass and 50 kWh/t for torrefied biomass.

Unit	Description
Pressurised injection (lock-hoppers for EF gasifier)	Inert gas for pressurisation: 0.5 $kgCO_2/kg_{B00}$, gas entrained in the gasifier: 0.2 $kgCO_2/kg_{B00}$, electricity consumption: 0.2 kJ/kg_{B00} extra, inert gas overpressure 5 bar. CO_2 is recycled from the acid gas removal step, the CO_2 which is not entrained in the gasifier is considered not recoverable.
EF gasifier	Steam and oxygen blown directly heated EF gasifier for which thermodynamic equilibrium is assumed. The S/B ratio is fixed, whereas the oxygen to biomass ratio is defined by the heat required to carry out the gasification reaction (direct heating). The gas species considered at equilibrium are H_2, CO, CO_2, H_2O, which make up most of the synthesis gas, and as CH_4, N_2, C_2H_4 and solid carbon, which are present in very small quantities.
FICFB gasifier	Steam blown indirectly heated fluidised bed gasifier. Modelled through a reactor where the atomic balances are defined by the set of equations and parameters described in detail in Section 1.2. The S/B ratio is fixed. The residual char (solid carbon) is separated through cyclones (not modelled) and combusted to provide heat. The heat loss is fixed at 10% of the heat required for gasification (equivalent to 1-2% of the LHV of the inlet biomass).

[a] Grinding is taken into account only for the EF gasifier options, as biomass is considered available in the form of wood chips which can be directly used in an FICFB gasifier. The electricity consumption depends also on the technology, the type of biomass, its moisture content etc.

Table 6: Synthesis gas conversion modelling and other models summary

Unit	Description
High Temperature Stage (HTS)	Gibbs Reactor, oxygen input to reach desired temperature, T_{HTS}= 1300 °C ([27]).

Unit	Description
Tar (catalytic) reformer	Dolomite guard bed and steam reforming Ni catalyst. WGS reaction to equilibrium, 80% CH_4 conversion, 90% C_2H_4 conversion, heavier tars and organic compounds are considered completely converted. Steam is added to obtain an S/C ratio of 2.5. CO_2, recycled from the AGR is added to obtain the desired H_2/CO ratio for F-T synthesis. Heat is provided through heat exchange (indirect heating). T_{CTR}=870 ℃. N.B.: Using this option excludes the WGS unit [28, 29].
Water Quench	Water is added with an overpressure of 12 bar and 20% is shifted, the WGS is considered the only reaction occurring in the quench. The outlet temperature is fixed at T_{wq} 750 ℃. In principle the synthesis gas can be cooled down to 150 ℃ (the inlet temperature for cold gas cleaning) in a total quench.
Gas Quench	The gas recycling ratio is fixed at 30%, the gas is cooled in a heat exchanger to 315 ℃. The compressor power consumption is estimated at 4.8 kW/kg$_{gas}$ (data from the Shell EF Gasifier taken as example, from the report by [30]).
Radiant panels	Heat exchanger cooling the synthesis gas to 800 ℃, heat is considered recoverable (with a $\Delta T_{min}/2 = 25$).
Oxygen production	Black-box model. The electrical energy required for the production of oxygen at purity (P_{oxy}) 99.5%$_{O_2}$ is set to 1080 kJ/kg ([31]). The electric energy required for 85%$_{O_2}$ $< P_{oxy} <$ 99.875 %$_{O_2}$ is obtained by fitting the data by [32].
Hot Gas Clean-up	Heat exchanger cooling the gas from ~ 800 ℃ to 400 ℃, heat is recoverable [27].
Cold Gas Clean-up	Cooling to 150 ℃, filter modelled as a 0.1 bar pressure drop and heat loss (to 25 ℃), stream is flashed to remove water [27].
Synthesis gas compression	Pressure ratio set to 3, interstage cooling to 35 ℃ with water separation.

Unit	Description
Water Gas Shift	Carried out at the same pressure as the synthesis of fuels, P_{syn}, only part of the stream is shifted with S/C ratio of 2.5 and overall outlet H_2/CO ratio is set at 2.1 (for FT synthesis). T_{wgs} = 250-320 ℃.
Steam Electrolysis	Model based on the work by [20, 21] described in Section 1.3. The model takes into account ohmic, diffusion and activation losses. The current density is set to j=0.3 A/cm^2 and the pressure to P_{SOEC}=1.5 bar. The model computes the operating voltage of the cell (V_{cell}) and the stack (V_{stack}), the electric power required (W_{el}), the total area (A_{stack}) and the heat and material balances of the unit operation. Hydrogen is compressed with interecooling to P_{syn}.
Co-electrolysis (CO_2 and steam)	The RWGS reaction at equilibrium is added to the steam electrolysis model under the assumption that the RWGS is much faster than the electrolysis of CO_2. The CO_2 is recycled from the AGR, the recycled fraction R_{CO_2} imposes the amount of CO_2 fed to the unit. The gas is compressed with intercooling to P_{syn}.
AGR	Black-box model representing amine scrubbing. Heat Duty 3.3 MJ/kgCO_2 at 150 ℃, of which 20% is recoverable from 90 to 40 ℃. Electricity requirement is fixed at 25 kJ$_e$/kgCO_2 [33], 95% of CO_2 is removed ([27, 34]) along with 95% of water.
Low Temperature F-T Synthesis	Co-catalyst as a reference, H_2/CO=2.1, α_{ASF} = 0.95 (0.85-0.95) ([35]), C1-C4 redistributed: C1 = 74%$_{mol}$, C2 = 16 %$_{mol}$, C3 = 6%$_{mol}$, C4 = 4%$_{mol}$ ([36, 31, 37]), olefin to paraffin ratio C2-C4 = 0.9, C5-C12 = 0.27, C13-C18 = 0.048 ([38]). Operating Temperature: T_{FT} = 180-250 ℃, Operating Pressure: P_{FT} = 25 bar. Once through CO conversion: 0.7-0.9 (0.8), up to 0.95, by imposing the fraction of internal recycle of unconverted gas R_{FT}.
F-T Upgrade	Black-box model, private data.
Compressors	Isoentropic efficiency = 0.8
Gas turbine	Isoentropic efficiency = 0.8
Pumps	Volumetric efficiency = 0.8

Unit	Description
Steam Network with steam turbines	[3, 4]

2. Appendix B: Economic modelling

The objective of the economic modelling is to determine the capital investment of a project and ultimately estimate its profitability for comparison between alternative options. The nomenclature, the methodology and all the assumptions used in this study to evaluate process profitability are described in detail in the following sections.

2.1. The capital investment

The capital investment cost estimates proposed in this study are to be considered prospectives, for the N^{th} plant on a greenfield site, and with an (optimistic) accuracy of about $\pm$ 30% (but that could prove even higher).

The first step in the evaluation is the estimation of the purchase cost, C_p, of the main equipment. When possible the purchase cost is estimated using empirical correlations provided by [39] and [40]. The purchase cost of the equipment built in carbon steel and operating under atmospheric pressure can be generally expressed in the form of Equation 27.

$$logC_p^0 = K_1 + K_2 \cdot logA + K_3(logA)^2 \tag{27}$$

K_i are parameters fitted from market studies and A is the relevant sizing parameter (for example the surface area for a heat exchanger and the power for a compressor). From the purchase cost it is possible to estimate direct (equipment, material, labour) and indirect (freight, overhead, engineering) costs relative to the installation of each piece of equipment, as shown in Equation 28. In the nomenclature used by [39], this corresponds to the *'bare module' cost* of each piece of equipment.

$$C_{BM} = C_p^0 \cdot [B_1 + B_2 \cdot F_p \cdot F_M] \tag{28}$$

B_1 and B_2 are constants depending on the type of equipment. The effect of the operating conditions (pressure and materials) is taken into consideration by the coefficients F_p and F_M.

For non standard equipment and for certain unit operations, the empirical correlations presented in Equation 27 and Equation 28 may not be available. Therefore, for these cases, the capacity factor method is employed (Equation 29). With this method the cost of the equipment is estimated considering a similar unit for which literature data is available. The corresponding 'bare module' cost of the equipment can then be estimated by Equation 29.

$$C_{BM} = C^0_{ref} \cdot \left(\frac{A}{A^0_{ref}} \right)^{exp} \cdot I_F \tag{29}$$

C^0_{ref} and A^0_{ref} represent the base cost and relative relevant sizing parameter from the literature. exp is the extrapolation factor which, if no further information is available, is assumed to be 0.7. I_F is the installation factor, representing the costs relative to the installation of the equipment (for example labour and freight). It is considered 1 if these costs are included in the reported base cost C^0_{ref}.

In this study, the sum of the 'bare module' cost of all the core equipments is considered as the InSide Battery Limit Equipments (ISBL)s.

$$ISBL = \sum_i (C_{BM_i} \cdot I_{act_i}) \tag{30}$$

The actualisation factor I_{act_i} takes into account the current cost and is expressed by the ratio of the Marshall & Swift cost index (M&S) today and at the time relative to the purchase estimate.

The additional costs to estimate the fixed capital costs are usually calculated starting from the ISBLs [41]. The build-up of the fixed capital considered in this study is summarised in Table 7.

Table 7: Cost build-up of the fixed capital costs (adapted from [41])

Utilities & Control	0.15 of ISBL
Storage & Spare parts	0.25 of ISBL
Engineering	0.20 of ISBL
Buildings & infrastructure	0.15 of ISBL
Licences	neglected
Contingencies	0.25 of ISBL

The expenses associated with the initial loads[3], the start-up, the working capital and the financial costs during construction are neglected in this study. This assumption is for consistency with previous studies, and because these costs are not generally mentioned in prospective techno-economic evaluation with a level of detail comparable to the one of this study. As mentioned earlier, the accuracy aimed at in this study is of ± 30%. The total investment cost is represented by the fixed capital costs, or CAPital EXpenditure (CAPEX), is referred to as the *depreciable capital* and it affects the operating costs, or OPErational EXpenditure (OPEX), as explained in the next section.

2.2. The operating costs

The operating costs can be divided into two parts:

- fixed cost (FC) - Do not directly depend on the production level. They include depreciation of the total investment costs and financial costs, maintenance and labour costs, property tax, insurances and general expenditures;
- Variable Costs (VC) - Directly depend on the production level. They include utilities (electricity, oxygen) costs, raw materials (biomass). Variable costs can be reduced by the sale of by-products (such as electricity).

The *fixed costs*, excluding depreciation and financial costs, referred to hereafter as FC^* for practical purposes, are assumed to be linear with the investment, as summarised in Table 8, under the assumption that the plant operates continuously.

Table 8: Assumptions for the yearly FC, without depreciation and financial costs, referred to as FC^* (adapted from [41])

General expenditures (ge)	0.01 of ISBL with controls & utilities
Maintenance Costs (m)	0.04 of ISBL with controls & utilities
Labour (l)	0.01 of ISBL with controls & utilities
Property tax & insurance (t&ins)	0.02 of ISBL with controls & utilities

The *variable costs* represent the costs that directly depend on the operating conditions, in this study, biomass and if required, natural gas, electricity and oxygen. Electricity and oxygen, in

[3]Catalyst costs are included in the equipment costs.

certain configurations of a BTL plant, can be sold as by-products. The selling price and buying costs assumptions are reported in Table 10.

2.2.1. Production cost

The production costs are the operating costs referred to the unit of product, which in the present case is defined as a litre of F-T fuel. The yearly production volume of F-T fuels, V_{F-T}, is calculated assuming that the BTL plant operates continuously during the year (considering for plant availability). Storage facilities are therefore necessary to stock biomass and assure operation and take into account the seasonal nature of biomass production.

For the sake of comparison with the literature,and in particular with the survey proposed by [41], a simplified estimate of the production costs (P^*), independent of the year of operation, is considered. The FC in this case are calculated assuming overnight construction, the economic and technical lifetimes are identical, investment is entirely provided by bank loans therefore the annuity is calculated as defined in Equation 31), depreciation is not taken into account.

$$Annuity = \frac{CAPEX}{\beta} \tag{31}$$

$$\beta = \frac{(1+DR)^{t_{tech}} - 1}{DR \cdot (1+DR)^{t_{tech}}}$$

The simplified estimate of the OPEX, OPEX*, is independent of the year or time period of operation, therefore P^* can be estimated according to Equation 32.

$$P^*_{fuel} = \frac{OPEX^*}{V_{F-T}} \tag{32}$$

2.3. Economic evaluation assumptions

In this section, the base assumptions considered for the economic modelling are summarised. Table 9 presents the assumptions relative to the evaluation of the capital investment. The reference unit used for the capital investment is the M€. As several equipment costs are available in US$ the exchange rate used, after actualisation, is provided. Given the high variability of currency exchange

rates, the values considered are calculated from the yearly average for 2010, 2011 and 2012 (from [42]). As mentioned before, the year index considered for consistency with previous studies, is the M&S and the values reported refer to 2011 (more recent information was not available for this study). Considering the evolution of other indexes, such as the IHS CERA Downstream Capital Costs Index (DCCI) and the Chemical Engineering Plant Cost Index (CEPCI), there is only a slight change between 2011 and 2012, with a 0.3% increase for the former and a 0.2% decrease for the latter. It is therefore acceptable to consider the estimates provided in this study valid for the years 2011 and 2012.

Table 9: Economic modelling financial assumptions: evaluation of the capital investment (adapted from [41])

Plant availability	0.9
Discount rate (DR)	0.07
Technical lifetime (t_{loan})	20
Exchange rate (US$ to €)	0.753
M&S	1536.5
DCCI	198.0
CEPCI	584.6
Reference Year	2011-2012

The electricity prices are the average values for the European Union and are calculated from the data available from [43]. The electricity and natural gas costs represent the average end-users' cost for industrial consumers. Green electricity represents the average feed-in tariff for electricity produced from biomass. Even though biomass is already traded on a global scale, a global market for biomass does not yet exist and therefore its price can vary greatly between studies. The price of biomass will depend on the location of a prospective BTL plant, on the type of biomass available and on its moisture content. Biomass price in literature studies varies between 3 and 10 €$_{2011}$/GJ [41]. In the current study, an average biomass price of 7 €/GJ is considered. Table 10 presents the assumptions relative to the evaluation of the operating costs.

Table 10: Economic modelling assumptions: cost of by-products and raw materials

Electricity price	100.5	€/MWh
Green electricity	119.69	€/MWh
Natural Gas	41.98	€/MWh
Biomass	7	€/GJ

Unless otherwise specified, only one electricity counter is assumed. That is, the electricity

produced is used by the process and only the net electricity is either bought at the electricity price or sold at the green electricity price.

2.4. Equipment sizing and costing

The cost estimation is carried out, when possible, using the empirical correlations by [39] and [40]. These correlations allow the estimate of the bare module cost of the main equipment as a function of the operating conditions and the relevant sizing parameter. For non-standard equipment, this approach is not possible and costs are evaluated on the basis of literature values using capacity-factored estimates (reported in Table 13). Because different studies use different nomenclatures and assumptions, it is often difficult to coherently use these estimates and therefore some assumptions are necessary to adapt, as far as possible, the costs to the current context. The costs are intended here as bare module costs, that is, as the installed costs of each unit operation. Their sum is used to evaluate the capital investment, as described in detail in Section 2.

The volume of reactors and vessels is often used as the relevant sizing parameter for estimating the cost. Assuming a cylindrical shape, the volume can be determined as a function of the average gas velocity, u_{mean} [m/s], or the residence time, τ [s]. When u_{mean} is known, the diameter, d [m], can be estimated according to Equation 33.

$$d = 2 \cdot \sqrt{\frac{\dot{V}}{u_{mean} \cdot \pi}} \tag{33}$$

$\dot{V}$ is the volumetric flowrate [m^3 s^{-1}]. The height h of the vessel/reactor can be calculated by considering a fixed ratio over d, or if available, by considering an exponential relationship with $\dot{V}$, fitted on data from commercial equipment, from [39, 40].

$$\frac{h}{d} = R_{h/d} = cst \tag{34}$$

$$h = h_0 \cdot \dot{V}^n \tag{35}$$

When the residence time τ is known, assuming $R_{h/d}$ constant, d can be estimated according to

Equation 36.

$$d = \sqrt[3]{\frac{\dot{V} \cdot \tau \cdot 4}{R_{h/d} \cdot \pi}} \tag{36}$$

The number of units is generally estimated by considering the constraints imposed by the maximum diameter d_{max} [m] (or volume V_{max} [m^3]) of the reactors/vessels. The underlying assumptions of this simple sizing procedure are that u_{mean} and τ remain constant with the scaling of the equipment.

2.4.1. Pretreatment

The pretreatment section includes a storage facility, a drying and/or torrefaction unit and for the options using an EF gasifier, a grinder. The storage facility and the grinder are priced according to the factor estimates relationships proposed by [31], based on the rate of biomass that is processed, as reported in Table 13.

Drying and torrefaction are carried out in a rotary dryer such as the Standard Turbo-Dryer® proposed by [44]. The torrefaction reactor and dryer are sized on the basis of their volume, which is calculated considering that the density of treated wood-chips is 300 kg/m^3, the wood to reactor volume ratio is 0.1 [$m^3_{wood}/m^3_{reactor}$], τ is 30 minutes for drying, 90 minutes for drying and torrefaction; the maximum reactor volume, V_{max}, is 950 m^3 and the height to diameter ratio, $R_{h/d}$, is set to 2. The relationship between size and cost reported in Table 13 is obtained from generic budget estimates provided by [44]. The estimates do not take into account the external loop for the recycling of the hot gases. The loop includes the vent designed to remove the water vapour and volatiles, the external indirect heater designed to introduce enough heat into the system to maintain the operating temperature, and a recirculating fan. The recirculating fan is priced through an empirical relationship for centrifugal fans based on power and considering cast steal as the construction material. The other components and the installation of the drying/torrefying equipment are taken into account assuming an installation factor, I_f, of 1.5.

2.4.2. Gasification

The EF gasifier is priced using the capacity-factor relationship proposed in the report by [45] and reported in Table 13. A train factor of 0.9 is assumed when several gasifiers are required at the same site [46]. The EF gasification unit operation also includes the oxygen compressor priced

through the empirical relationship for centrifugal fans based on their power. The FICFB gasifier is priced by sizing the gasification and combustion chambers and considering the empirical volume - price relationship for fluidised beds reported, as previously done by [1, 5]. As in the previous studies, a multiplication factor of 4 is introduced to estimate the cost of the FICFB gasifiers, which takes into account the new technology relative to biomass gasification ([5]). The sizing parameters for the gasifiers are summarised in Table 11.

Table 11: Gasifiers sizing parameters summary

Unit	τ [a]	u_{mean} [a]	$R_{h/d}$	h_0 [a]	n [a]	Max size
EF gasifier	2 s		10			432 MW_{th} [b]
FICFB gasification chamber		0.645 m/s		4.07	0.188	d_{max}=10 m [c]
FICFB combustion chamber		5.45 m/s		8.47	0.188	

[a] As reported by [5].
[b] The maximum capacity used as a reference is the installed capacity considered by [45].
[c] The maximum diameter is considered here as an assumption, based on the size of fluidised beds available in the oil refining industry. For example, the diameter of fluidised bed catalytic cracking reactors can be in the range of 10-15 m [47].

Both configurations use a centrifugal pump and bucket conveyor. The centrifugal pump is used to supply the water which is then converted into steam and the bucket conveyor is used for the transport of biomass. The centrifugal pump is priced based on its power from an empirical correlation. The size of the bucket conveyor is considered as three times the height of the gasifier based on data from the Güssing plant ([5]) and its cost is estimated using the corresponding empirical correlation.

The gasification section includes tar removal and synthesis gas cooling unit operations. The synthesis gas produced by the EF gasifier is considered tar free because of the high operation temperature. The tars present in the synthesis gas produced by the FICFB gasifier can be thermally cracked (in the high temperature stage) or catalytically reformed (tar reformer). Both unit operations are priced considering capacity-factored estimates reported by [31] and by [28] respectively, and presented in Table 13. The sizing of the catalytic tar reformer is based on the assumption that the Gas Hourly Space Velocity (GHSV) (2476 hr^{-1}) , reported in the techno-economic evaluation by [28], remains constant with scale.

The synthesis gas cooling can occur through a direct water quench, a high temperature heat

exchanger or a gas quench. The water quench and the high temperature heat exchanger are priced through the capacity-factored estimates reported by [46] and by [31] respectively, and presented in Table 13. The gas quench is represented by a high temperature heat exchanger, priced with the same capacity factor used by [31], and a centrifugal compressor, priced with an empirical relationship and considering stainless steel as the building material.

The parameters for the sizing and cost estimation of the major equipment belonging to the gasification section and priced according to empirical relationships by [39] and [40], are summarised in Table 12.

Table 12: Gasification section sizing and pricing parameters summary

Equipment	Material	Pressure
Oxygen compressor (EF gasifier) [a]	Carbon steel	1 bar
Gasification chamber (FICFB gasifier)	Nickel alloy	1 bar
Combustion chamber (FICFB gasifier)	Nickel alloy	1 bar
Centrifugal Pump (water feed)	Carbon steel	1 bar
Bucket conveyors		1 bar
Centrifugal compressor (gas quench) [a]	Stainless Steel	$\approx$ 28 bar

[a] Isoentropic efficiency = 0.8

It should be underlined that, because biomass gasification units do not currently exist in relevant capacities, the estimate of their prospective cost is particularly difficult and affected by uncertainty.

2.4.3. Oxygen production

Oxygen production can be considered on-site, in the case where an Air Separation Unit (ASU) is built along the BTL plant, or off-site, in the case that oxygen is bought as a utility. Its price is determined by the technology used for production, which in turn depends on the required flowrate. The relationship between mass flowrate and price (and technology) is considered from the work by [48] as was done in the previous studies by [27] and [1]. The price of oxygen varies between 0.03 €$_{2011}$/kg and 0.7 €$_{2011}$/kg (1-10^5 m^3/h) ([48]). If the ASU is on-site, the associated investment cost is considered using the capacity-factored estimate, on the basis of the oxygen production rate by [31], as reported in Table 13. The unit is a cryogenic ASU providing oxygen at 99.5% purity.

2.4.4. Gas cleaning and adjustment

After the removal of tars, the composition and pressure of the synthesis gas are adjusted to satisfy the requirements of the fuel synthesis section. Other contaminants are removed and the H_2/CO ratio is increased if necessary. The contaminants can be removed using conventional wet scrubbing (cold gas cleaning) or advanced dry technology (hot gas cleaning). The hydrogen content is adjusted either through WGS or by adding H_2 produced in a high temperature SOEC.

Cold gas cleaning includes cyclones and a bag filter for residual gas removal, and a wet scrubber. Its cost is estimated on the basis of the capacity factor correlations by [31]. In the hot gas cleaning unit operation contaminants are removed through chemical absorption at high temperature. Its cost is also estimated on the basis of the assumptions by [31]. The relationships for cold and hot gas cleaning components are based on the flowrate of processed gas and are reported in Table 13.

In the case of atmospheric gasification (for FICFB gasification), the clean synthesis gas is compressed in a multi-stage compressor, priced according to empirical relationships assuming 0.8 isoentropic efficiency and carbon steel as the construction material.

The WGS reactor is considered as a single stage shell and tube heat exchanger. The procedure for its sizing and price estimation is described in detail by [5] on the basis of the work by [49]. The cost of the reactor and the cost of the catalyst are calculated, through empirical relationships, as a function of the reactor pressure, the total flowrate of the gas, as well as the flowrates of CO and H_2O, and the CO conversion.

The cost of the high temperature electrolysis and co-electrolysis units, the SOEC, is considered from the report by [50]. The cost per square metre of electrolyser includes the autoclave, the electric equipment, the electrolyser itself and installation ([50]). It is assumed that the electrolyser is replaced every five years. For simplicity, this cost is accounted for, without discount, at the beginning of the lifetime of the plant. The costs are reported in Table 13. The cost of a centrifugal compressor (with isoentropic efficiency of 0.8) is added to the unit cost, as the SOEC operates at atmospheric pressure and the H_2 is compressed to the operating pressure of the synthesis step.

2.4.5. Acid gas removal

The AGR unit operation consists in an amine scrubber, capable of removing CO_2 and $H2_S$ from the main process gas stream. Its cost is determined from the report by [28]. This study specifies the base cost and exponential factor for scaling, but not the base variable, nor its units. Here, it is assumed that the base variable for scaling is the amount of separated CO_2 reported in the process flow diagrams.

2.4.6. Fuel synthesis and upgrading

The F-T fuel synthesis is priced according to the estimate by [37] for a Co-catalyst, low temperature, multitubular fixed-bed reactor (of the type developed for the Shell Middle Distillate Process). The capacity-factored estimate is based on the molar flow of the synthesis gas at the inlet of the reactor. The upgrading section cost is estimated on the basis of an hydrocarbon processing unit, scaled on the F-T fuel produced. The estimates are shown in Table 13.

2.4.7. Power recovery

Power recovery for electricity co-production includes the heat exchanger network, the steam turbines, and the gas turbines.

The heat exchanger network cost is determined from the heat exchanger area and the minimum number of heat exchangers required to satisfy the energy target computed by the process integration algorithm, as outlined by [51]. The average area is used to estimate the price of the heat exchangers through the empirical correlations by [39] relative to fixed tube sheet units. It is assumed that the heat exchangers are equally distributed between units in nickel alloy, operating at high pressure, and in carbon steel, operating at low pressure. This simplified procedure generally overestimates the cost of a heat exchanger network with the same total area and number of heat exchangers [52].

The costs of the steam turbines and gas turbines are determined based on their shaft power and including electric drives according to the corresponding empirical correlations by [39].

2.5. Summary of capacity-factored cost estimates

The summary of the costs determined through capacity-factored estimates (Equation 29, in Section 2) is presented in Table 13 from cost data obtained from literature. The reference costs used

may incorporate installation costs, direct and indirect costs associated with the investment. The base costs and corresponding installation factor, I_f, were back-calculated to deliver the bare module cost of each unit, that is, its contribution to the ISBL. This was done, when possible, considering the build-up of the investment of the reference study and, if it was not available, the one presented in this study in Table 7 in Section 2. I_f is therefore not equivalent to the 'overall installation factor' which is sometimes used in the literature and includes direct and indirect expenses.

Table 13: Units for which the investment is calculated using capacity-factored methods. Costs are in €$_{2012}$.

Unit	base cost Cp_0	base unit	base A_0	scale exp	installation I_f	max size
Drying and torrefaction units[a]	17370 €	m^3	1 m^3	0.74	1.5	920
Grinding	0.48 M€	$t_{in,ar}$/hr	33.5	0.6	1	110
Storage	1.16 M€	$t_{in,ar}$/hr	33.5	0.65	1	110
EF gasifier[e]	54.59 M€	MW_{th}	432	0.7	1	432
High-temperature electrolysis[b]	5574 €	$m^2_{electrolyser}$	1	1	1	-
Electrolyser replacement[c]	1306 €	$m^2_{electrolyser}$	1	1	1	-
Air separation unit (99.5%$_{O_2}$)[d]	29.11 M€	tpd	576	0.75	1	3200
Quench (direct)[f]	326 k€	$m^3_{in,gas}$/s	3.743	0.7	3	3.743
High-temperature heat exchanger[d]	8.45 M€	MW_{th}	138.1	0.7	1	-
High-temperature stage	3.76 M€	$m^3_{in,gas}$/s	34.2	0.7	1	-
Tar reformer[g]	3.25 M€	m^3	76.2	0.65	1.39	-
Tar reformer catalyst regenerator[g]	3.64 M€	m^3	76.2	0.65	1.39	-
Cyclones[d]	3.13 M€	$m^3_{in,gas}$/s	34.2	0.7	1	180
Bag house filter[d]	1.98 M€	$m^3_{in,gas}$/s	12.1	0.65	1	64
Wet scrubber[d]	3.13 M€	$m^3_{in,gas}$/s	12.1	0.7	1	64
Dry cleaning[d]	35.80 M€	$m^3_{in,gas}$/s	74.1	1	1	-
AGR[h]	4.54 M€	kmolCO_2/h	542	0.75	1.39	-
F-T Multitubular Fixed Bed[i]	11.21 M€	$kmol_{in,gas}$/s	0.9025	0.67	1	-
Upgrading[l]	86.66 M€	$t_{FTcrude}$/h	333.3	0.7	1	-

[a] Cost relationship regressed from data obtained from [44], assuming wood to reactor volume ratio 0.1 [m^3_{wood}/m^3_{unit}]. Valid starting from a volume of 115 m^3.
[b] Installed costs, include electric equipment and thermal insulation ([50]).
[c] Includes labour costs for installation. It is assumed that the electrolyser is replaced every 5 years ([50]).
[d] Adapted from [31].
[e] Adapted from [45].
[f] Adapted from [46].
[g] Adapted from [28], cyclons are included. The reference base unit is not specified, it is presumed here to be the reactor volume.
[h] Adapted from [28]. The reference base unit is not specified, it is presumed here to be the CO_2 separated by the amine scrubber.
[i] Adapted from [37], referring to SMDS-synthesis process.
[l] Private.

3. Appendix C: Complementary figures

The results obtained minimising the CAPEX and maximising the η_{eq} of the BTL conversion process are represented in terms of η_{en} and η_{chem}, with respect to the CAPEX in Figures 8 and 9. Figure 8 presents the η_{en}, with respect to the CAPEX showing that all optimised solutions belong to the 0.4 - 0.6 η_{en} range. The η_{en}, therefore, does not highlight the trade-offs between different solutions for the BTL process. The trade-off is clear when considering the η_{chem} with respect to the CAPEX, which is presented in Figure 9. The increase in η_{chem} is strongly related to the increase in CAPEX. It should be highlighted, however, that this indicator does not take into account the electricity requirement or co-production of the different processes.

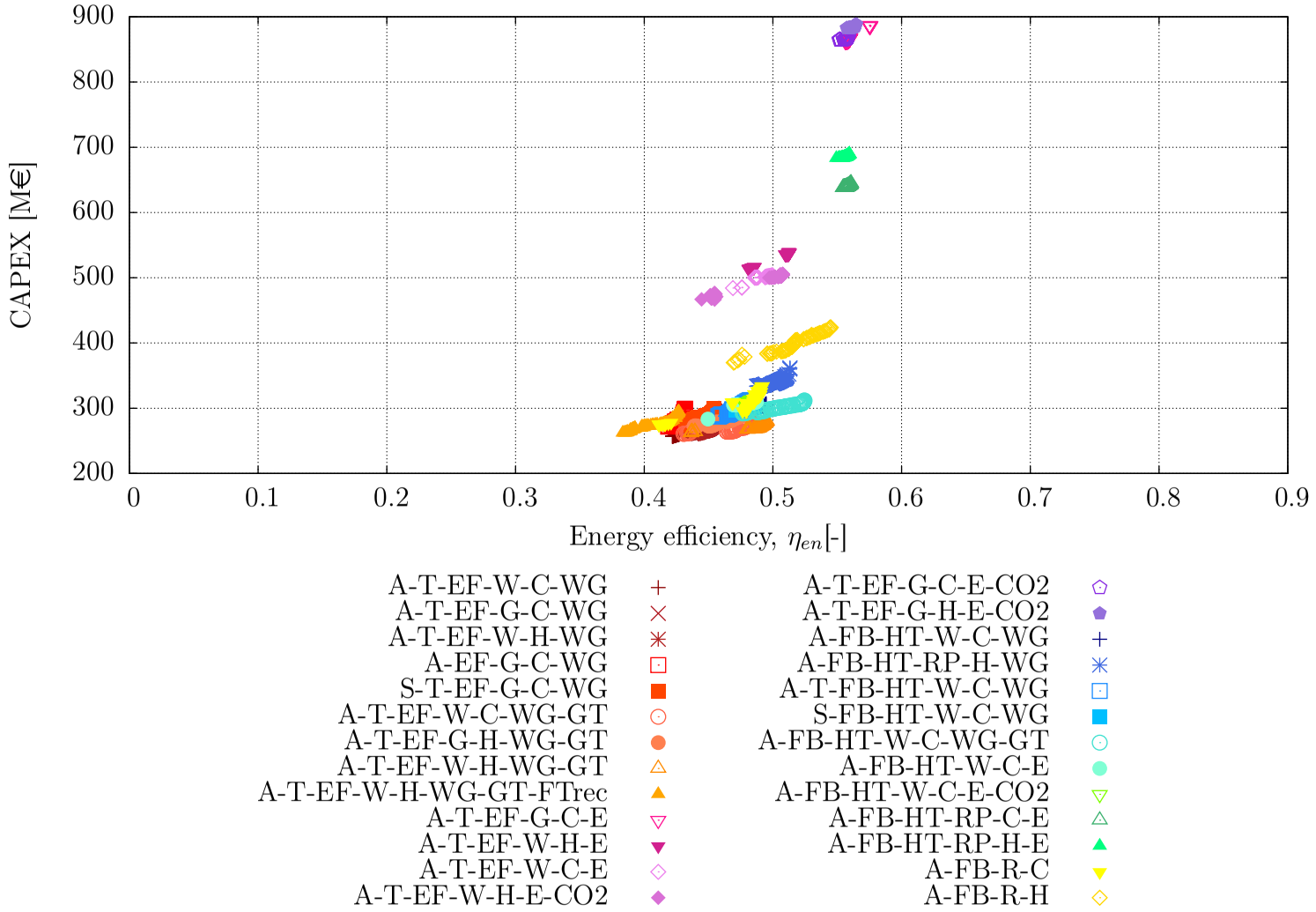

Figure 8: Energy efficiency (η_{en}) vs. CAPEX of the solutions obtained from the multi-objective optimisation of each scenario presented in the main article.

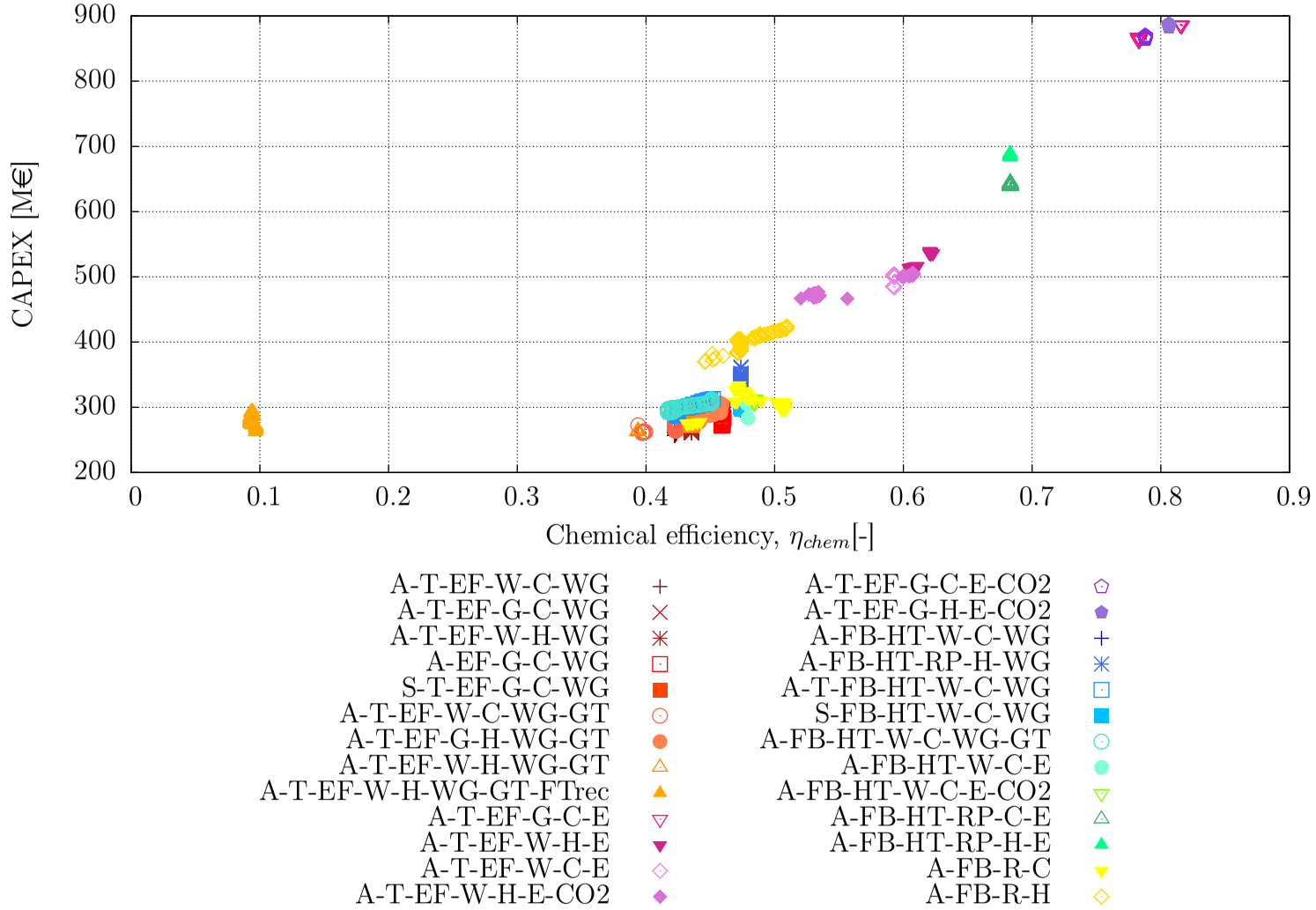

Figure 9: Chemical efficiency (η_{chem}) vs. CAPEX of the solutions obtained from the multi-objective optimisation of each scenario presented in the main article.

Bibliography

[1] M. Gassner, *Process design methodology for thermochemical production of fuels from biomass. Application to the production of synthetic natural gas from lignocellulosic resources*, École Polytechnique Fédérale de Lausanne, Switzerland, 2010.

[2] F. Maréchal and B. Kalitventzeff, *Computers & Chemical Engineering*, 1996, **20**, 225–230.

[3] F. Maréchal and B. Kalitventzeff, *Computers & Chemical Engineering*, 1998, **22**, S149—-S156.

[4] F. Maréchal and B. Kalitventzeff, *Computers & Chemical Engineering*, 1999, **23**, s133–s136.

[5] L. Tock, *Evaluation Thermo-économique des productions de carburants liquides à base de biomasse*, École Polytechnique Fédérale de Lausanne, Switzerland, 2009.

[6] S. Pierucci and E. Ranzi, *Computer Aided Chemical Engineering*, 2008, **25**, 901–906.

[7] G. Schuster, G. Löffler, K. Weigl and H. Hofbauer, *Bioresource Technology*, 2001, **77**, 71–79.

[8] M. Baratieri, P. Baggio, L. Fiori and M. Grigiante, *Bioresource technology*, 2008, **99**, 7063–73.

[9] M. J. Prins, K. J. Ptasinski and F. J. Janssen, *Energy*, 2007, **32**, 1248–1259.

[10] J. Kalina, *Chemical and Process Engineering*, 2011, **32**, 73–89.

[11] R. T. Ng, D. H. Tay, W. A. Wan Ab Karim Ghani and D. K. Ng, *Applied Thermal Engineering*, 2013, **61**, 98–105.

[12] I. Hannula and E. Kurkela, *Biomass and Bioenergy*, 2012, **38**, 58–67.

[13] W. Gumz, *Gas Producers and Blast Furnaces: Theory And Methods of Calculation*, John Wiley & Sons, 1950.

[14] M. Gassner and F. Maréchal, *Biomass and Bioenergy*, 2009, **33**, 1587–1604.

[15] S. Valin, S. Ravel, J. Guillaudeau and S. Thiery, *Fuel Processing Technology*, 2010, **91**, 1222–1228.

[16] Belsim S.A., *Belsim Vali*, 2013, www.belsim.com.

[17] F. Kirnbauer, V. Wilk, H. Kitzler, S. Kern and H. Hofbauer, *Fuel*, 2012, **95**, 553–562.

[18] S. Valin, *Personal communication*, 2013.

[19] H. Hofbauer and R. Rauch, Progress in Thermochemical Biomass Conversion, Innsbruck, Austria, 2000.

[20] J. Van herle, F. Maréchal, S. Leuenberger, Y. Membrez, O. Bucheli and D. Favrat, *Journal of Power Sources*, 2004, **131**, 127–141.

[21] J. Van herle, F. Maréchal, S. Leuenberger and D. Favrat, *Journal of Power Sources*, 2003, **118**, 375–383.

[22] Q. Fu, C. Mabilat, M. Zahid, A. Brisse and L. Gautier, *Energy & Environmental Science*, 2010, **3**, 1382.

[23] W. A. Surdoval, ECS Transactions, 2009, pp. 21–27.

[24] W. Boie, *Energietechnik*, 1953, **3**, 309–16.

[25] E. Peduzzi, G. Boissonnet and F. Maréchal, *Fuel*, 2016, **181**, 207–217.

[26] E. Peduzzi, G. Boissonnet, G. Haarlemmer, C. Dupont and F. Maréchal, *Energy*, 2014.

[27] L. Tock, M. Gassner and F. Maréchal, *Biomass and Bioenergy*, 2010, **34**, 1838–1854.

[28] S. Phillips, A. Aden, J. Jechura, D. Dayton and C. Eggeman, *Thermochemical ethanol via indirect gasification and mixed alcohol synthesis of lignocellulosic biomass*, National Renewable Energy Laboratory Technical Report, 2007.

[29] C. Reyes Valle, A. Villanueva Perales, F. Vidal-Barrero and A. Gómez-Barea, *Applied Energy*, 2013, **109**, 254–266.

[30] National Energy Technology Laboratory, *Cost and Performance Baseline for Fossil Energy Plants Volume 1: Bituminous Coal and Natural Gas to Electricity*, U.S. Department of Energy Technical Report, 2010.

[31] C. Hamelinck, A. Faaij, H. Denuil and H. Boerrigter, *Energy*, 2004, **29**, 1743–1771.

[32] A. Darde, R. Prabhakar, J.-P. Tranier and N. Perrin, *Energy Procedia*, 2009, **1**, 527–534.

[33] S. Heyne and S. Harvey, *International Journal of Energy Research*, 2014, **38**, 299–318.

[34] S. Heyne, M. C. Seemann and S. Harvey, Chemical Engineering Transactions, 2010, pp. 409–414.

[35] A. de Klerk, in *Kirk-Othmer Encyclopedia of Chemical Technology*, John Wiley & Sons, Inc., Hoboken, NJ, USA, 2013.

[36] G. P. V. D. Laan, *Ph.D. thesis*, Rijksuniverisiteit Groningen, 1999.

[37] I. Hannula and E. Kurkela, *Liquid transportation fuels via large-scale fluidised-bed gasification of lignocellulosic biomass*, VTT Technical Research Centre of Finland Technical Report, 2013.

[38] F. Bertoncini, M. C. Marion, N. Brodusch and S. Esnault, *Oil & Gas Science and Technology - Revue de l'IFP*, 2009, **64**, 79–90.

[39] R. Turton, B. Richard C., W. Wallace B. and S. A. Joseph A., *Analysis, Synthesis, and Design of Chemical Processes*, Prentice Hall; 2nd Edition, 2002, p. 987.

[40] G. D. Ulrich and T. V. Palligarnai, *Chemical Engineering Process Design and Economics, a Practical Guide [Hardcover]*, Process Publishing; 2nd edition, 2004, p. 706.

[41] G. Haarlemmer, G. Boissonnet, J. Imbach, P.-A. Setier and E. Peduzzi, *Energy & Environmental Science*, 2012, **5**, 8445.

[42] Fxtop, *Major historical exchange rates*, 2012, fxtop.com/en/historical-exchange-rates.

[43] Europe's Energy Portal, *Europe's Energy Portal*, 2012, www.energy.eu.

[44] Wyssmont, *Standard Turbo-Dryer*, 2014, www.wyssmont.com.

[45] A. Vogel, S. Brauer, F. Müller-Langer and D. Thrän, *Deliverable D 5.3.7 Conversion Costs Calculation. Project: RENEW - Renewable Fuels for Advanced Powertrains*, 2007.

[46] R. M. Swanson, A. Platon, J. A. Satrio, R. C. Brown and D. D. Hsu, *Techno-Economic Analysis of Biofuels Production Based on Gasification*, National Renewable Energy Laboratory Technical Report Supplement 1, Elsevier Ltd, 2010.

[47] G. Jiménez-García, R. Aguilar-López and R. Maya-Yescas, *Fuel*, 2011, **90**, 3531–3541.

[48] M. J. Kirschner, in *Ullmann's Encyclopedia of Industrial Chemistry*, Wiley-VCH Verlag GmbH & Co. KGaA, Weinheim, Germany, 2000, pp. 617–635.

[49] F. Maréchal, F. Palazzi, J. Godat and D. Favrat, *Fuel Cells*, 2005, **5**, 5–24.

[50] C. Mansilla, *Internal document*, CEA Technical Report, 2009.

[51] M. Gassner and F. Maréchal, *Computers & Chemical Engineering*, 2009, **33**, 769–781.

[52] S. Ahmad, B. Linnhoff and R. Smith, *Computers & Chemical Engineering*, 1990, **14**, 751–767.